Active deformation in Zagros-Makran transition zone inferred from GPS measurements

R. Bayer, J. Chery, M. Tatar, Ph. Vernant, M. Abbassi, F. Masson, F. Nilforoushan, E. Doerflinger, V. Regard, O Bellier

Geophys. J. Int. (2006) **165,** 373–381 doi: 10.1111/j.1365-246X.2006.02879.x

Active deformation in Zagros–Makran transition zone inferred from GPS measurements

R. Bayer,[1,*] J. Chery,[1] M. Tatar,[2] Ph. Vernant,[1,†] M. Abbassi,[2] F. Masson,[1] F. Nilforoushan,[3] E. Doerflinger,[1] V. Regard[4] and O. Bellier[4]

[1] *Laboratoire Dynamique de la lithosphere, University of Montpellier II-CNRS , Pl. E. Bataillon,* 34095 *Montpellier Cedex* 05, *France*
[2] *International Institute of Earthquake Engineering and Seismology, Farmenieh, Dibaji, Arghavan St., n°* 27, 19531, *Tehran, Iran*
[3] *Geodynamic Department, National Cartographic Center,* Po BOX 13185-1684, *Meraj Ave., Tehran, Iran*
[4] *CEREGE, University of Aix-Marseille III, Europole Méditerranéen de l'Arbois, BP* 80, 13545, *Aix en Provence, Cedex* 04*, France*

Accepted 2005 October 26. Received 2005 October 24; in original form 2004 September 14

SUMMARY

The Bandar Abbas-Strait of Hormuz zone is considered as a transition between the Zagros collision and the Makran oceanic subduction. We used GPS network measurements collected in 2000 and 2002 to better understand the distribution of the deformation between the collision zone and the Makran subduction. Analysing the GPS velocities, we show that transfer of the deformation is mainly accommodated along the NNW–SSE-trending reverse right-lateral Zendan–Minab–Palami (ZMP) fault system. The rate is estimated to 10 ± 3 mm yr^{-1} near the faults. Assuming that the ZMP fault system transfers the motion between the Makran–Lut Block and the Arabian plate, we estimate to 15 mm yr^{-1} and 6 mm yr^{-1}, respectively, the dextral strike-slip and shortening components of the long-term transpressive displacement. Our geodetic measurements suggest also a 10–15 km locking depth for the ZMP fault system. The radial velocity pattern and the orientation of compressive strain axes around the straight of Hormuz is probably the consequence of the subducting Musandam promontory. The N–S Jiroft–Sabzevaran (JS) fault system prolongates southwards the dextral shear motion of the Nayband–Gowk (NG) fault system at an apparent rate of 3.1 ± 2.5 mm yr^{-1}. The change from strong to weak coupling for underthrusting the Arabian plate beneath the Zagros (strong) and the Makran (weak) may explain the dextral motion along the ZMP, JS/NG and Neh–Zahedan fault systems which transfer the convergence from a broad zone in the western Iran (Zagros, Tabriz fault system, Alborz, Caucasus and Caspian sea surroundings) to Makran subduction.

Key words: active deformation, collision, GPS, Makran, Subduction, Zagros

1 INTRODUCTION

The present-day N–S convergence between the Arabian and the Eurasian plates is partially accommodated along the Zagros fold and thrust belt and the Oman oceanic lithosphere subduction. The Musandam peninsula-Bandar Abbas-Strait of Hormuz zone, also called the 'Oman line', is considered to be the transition between the Zagros continental collision and the Makran oceanic subduction (Kadinsky-Cade & Barazangi 1982) (Fig. 1). The Zendan–Minab–Palami (ZMP) faults accommodate the differential of velocity between the eastern Zagros and western Makran domains. This ZMP fault system runs west of the Makran accretionary wedge up to the Main Zagros Thrust area (MZT). Then, the differential of velocity between the Central Iranian Block (CIB) and the Lut block is taken up by the active Jiroft–Sabzevaran (JS) faults which are considered as the south prolongation of the Nayband–Gowk (NG) strike-slip system (Regard *et al.* 2004). GPS data in Iran have proved that Arabia converges towards Southeastern Iran at velocity of 23 ± 2 mm yr^{-1} near the western termination of the Makran subduction (Vernant *et al.* 2004), less than the time-averaged 36.5 mm yr^{-1} velocity proposed by the NUVEL 1 model (DeMets *et al.* 1990). Moreover, Tatar *et al.* (2002) have shown that Central Zagros accommodates 10 ± 4 mm yr^{-1} of NNE shortening. Based on a large scale GPS network Vernant *et al.* (2004) suggested a right-lateral strike-slip rate of $\sim$11 mm yr^{-1}. This rate is consistent with the recent geomorphic and tectonic analyses suggesting 11–13 mm yr^{-1} of right-lateral strike-slip motion over the whole ZMP and JS fault systems (Regard *et al.* 2004, 2005). Based on the comparison of the GPS velocity field deduced from the large scale Iranian Geodetic

*Corresponding author: DL laboratory, ISTEEM, case 060, Université Montpellier II, 4 place E. Bataillon 34095 Montpellier Cedex 05, France. E-mail: Roger.Bayer@dstu.univ-montp 2.fr.
†Now at: Department of Earth, Atmospheric and Planetary Sciences, Massachusetts Institute of Technology, Cambridge, MA, USA.

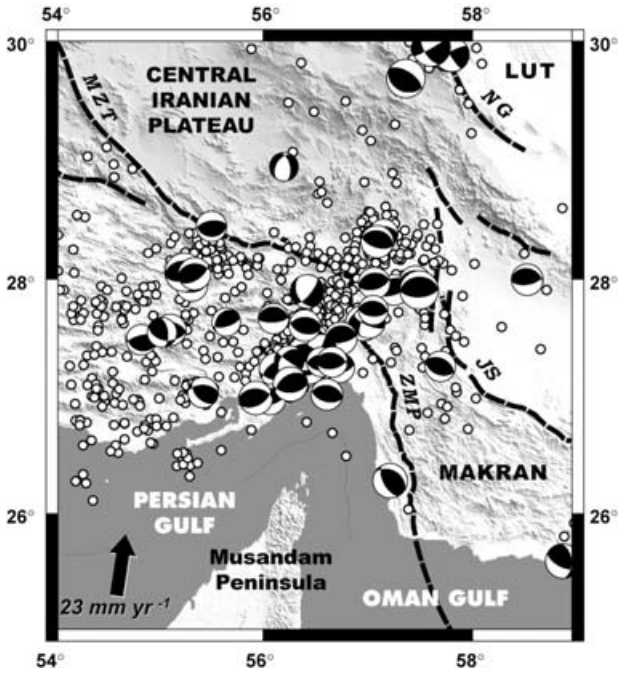

Figure 1. Earthquakes in the Zagros Makran transition zone. Seismicity from Engdahl's catalogue (Engdahl *et al.* 1998) and Harvard CMT solutions (*Harvard University Moment Tensor catalogue (CMT project) and data set available at http://www;seismology.harvard.edu/CMTsearch.html*). JS: Jiroft Sabzeveran fault system; ZMP: Zendan–Minab–Palami fault system; NG: Nayband-Gowk fault system; MZT: Main Zagros Thrust.

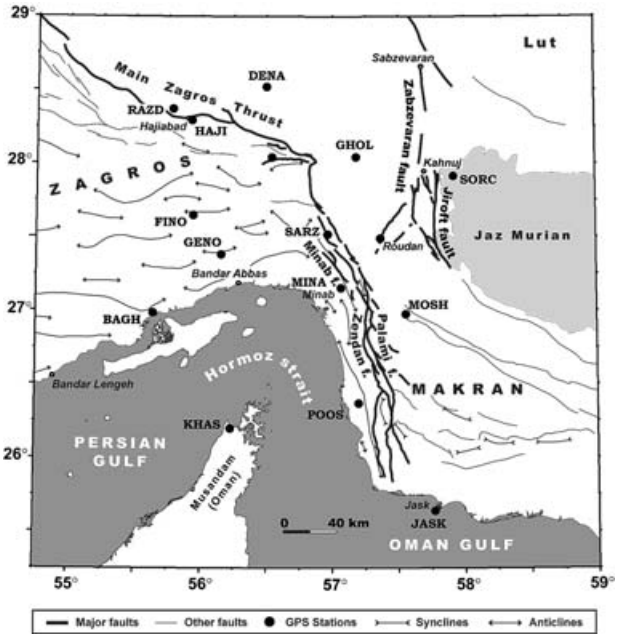

Figure 2. Simplified structural and tectonic map of the Zagros–Makran transition zone from Regard *et al.* (2004). Black filled circles indicate the location of the GPS sites. Note the sigmoid shape of the folds in the southeastern Zagros.

Network (Vernant *et al.* 2004), Masson *et al.* (2005) have recently suggested a low seismic strain rate/geodetic strain rate ratio over the Zagros–Makran transition zone. High geodetic strain rates and rotation of the compressive axis from N10° to N45° were evidenced, but the poor resolution of the GPS network (average benchmark spacing ∼300 km) prevented Vernant *et al.* (2004) and Masson *et al.* (2005) to go from examining details of the deformation in the Zagros Makran transfer zone. Accordingly, we implemented a dense geodetic network to map in detail the deformation and to understand the role of the ZMP and JS fault systems in the collision–subduction transfer. In this paper, we present the horizontal velocity distribution estimated from two GPS campaigns in 2000 and 2002. We consider the implications of the GPS motion on the tectonic structures of the southeastern Zagros and attempt to determine the strain distribution along the ZMP fault system.

2 TECTONIC AND SEISMICITY SETTINGS

The Zagros fold and thrust belt has been an active continental collision since the Neogene. It corresponds to a thick and deformed continental accretionary prism within the Arabian plate. Its southeastern termination coincides with EW-trending folds and thrusts (Blanc *et al.* 2003) crossed by NNW and NE strike-slip faults (Hessami *et al.* 2001). The SE Zagros shows very intense but low-magnitude seismicity. This seismicity is limited to the north by the Main Zagros Thrust (MZT) (Fig. 1). Several focal mechanisms are located at 8–14 km depth within the basement (Jackson & Fitch 1981; Baker *et al.* 1993). They are related to steep reverse faults with EW striking nodal planes and NE–SW-trending left-lateral displacement. To the north, the Central Iranian Plateau (CIP), called also Central Iranian Block, is considered to be a quasi-rigid block on the basis of seismological (Jackson & McKenzie 1988) and GPS observations (Vernant *et al.* 2004). To the East, the remnant Tethys oceanic lithosphere has been subducted northwards since the Cretaceous beneath the Makran coast, leading to the accretion of a large amount of subaerial and submarine sediments. The present-day seismicity of the Makran is low. Large magnitude events are related to the down going plate at intermediate depths or to superficial large historical earthquakes in eastern Makran (Byrne *et al.* 1992).

Between the Zagros and the Makran, the ZMP fault system is 20–30 km wide and 250 km long, and it is composed of three parallel faults (Fig. 2). The ZMP faults are linked to the MZT to the north and to the western end of the Makran prism to the south. It lines up with the Arabian continental shelf edge that borders the east side of the Musandam peninsula (Ravaut *et al.* 1997, 1998). The ZMP fault zone is characterized by strike-slip, oblique reverse and thrust faulting (Regard *et al.* 2004), and enlarges from a north single fault trace, the Zendan fault, to the south termination, the Zendan and Palami fault zone, which consist of numerous fault segments arranged in a horsetail pattern. Fault-slip analyses indicate a N45° trending compressive stress regime, which is oblique to the N10° trend of the Arabia–Iran convergence rate (Regard *et al.* 2004). Molinaro *et al.* (2005) have recently proposed that the MZT and the ZMP fault system are part of a single low-angle fault accommodating essentially dip-slip movement.

80 km to the East of the ZMP fault zone, the JS faults are characterized by a right-lateral strike-slip motion (Regard *et al.* 2004) similar to that for the Nayband and Gowk faults (Walker & Jackson 2002). The JS faults bend into an NW–SE orientation along the southern limit of the Jaz Murian depression (Fig. 2). Tectonic and geomorphic analyses combined with cosmonucleide dating have revealed a total right-lateral velocity of 4.7 ± 2.0 mm yr^{-1} or

6.3 ± 2.3 mm yr^{-1} for the Minab–Zendan fault system depending on age of fault offsets , and 5.7 ± 1.7 mm yr^{-1} for the JS fault system (Regard *et al.* 2005, see Table 3). The velocity of the JS fault system is larger than the 1.5–2.4 mm yr^{-1} proposed by Walker & Jackson (2002) for the Nayband fault on the base of a dated old volcanic lava flow offset by the fault.

The seismicity is mostly concentrated in the eastern Zagros and between the ZMP fault system and the JS fault zone in the north part of the transition zone (Fig. 1). Earthquakes reported by Kadinsky-Cade & Barazangi (1982) are located in the crust with a northeastward dip at 15–30 km depth, consistent with recent microseismicity studies (Yamini Fard *et al.* 2003). The focal mechanisms correspond to NE- trending reverse motions. This deep seismicity has been interpreted as a consequence of underthrusting of a wedge of Arabian shelf edge beneath Iranian crust or by the indentation of the Musandam Peninsula (Kadinsky-Cade & Barazangi 1982).

Contrasting with this northern zone, very low seismicity energy is released along the JS and ZMP fault zones. This is particularly the case for the ZMP fault zone south of latitude 27°N where only one teleseismic event ($Mw = 5.9$) was recorded in 1983 (*Harvard University Moment Tensor catalogue (CMT project) and data set available at http://www;seismology.harvard.edu/CMTsearch.html*). The focal mechanisms of the upper crustal events near the JS and ZMP fault zones, as for the 1983 earthquake, confirm the right-lateral component of the deformation along these two fault systems (Yamini Fard *et al.* 2003).

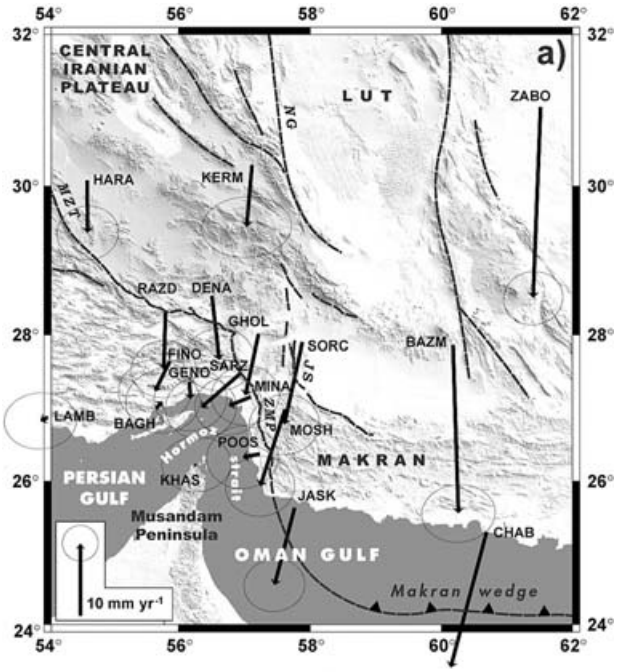

Figure 3. GPS horizontal velocities and their 95 per cent confidence ellipses estimated from GPS data collected during the 2000 and 2002 campaigns in Arabia fixed reference frame (a). Velocities estimated for the period 1999–2001 at sites of the Iran Global Network are also shown (Vernant *et al.* 2004).

3 GPS MEASUREMENTS AND DATA PROCESSING

The GPS network consists of 15 benchmarks over a 300 × 200 km domain spanning the Zagros–Makran transition zone (Figs 2 and 3). The mean distance between sites is 60 km. The network was measured using Ashtech Z12 receivers in 2000 January and again in 2002 January. For both epochs, each benchmark was measured for 48 hr except for a few reference stations permanently installed during the campaign (JASK, MINA, HAJI in 2000 and JASK, MINA, RAZD in 2002).

Data analysis was achieved using the same processing techniques as in Vernant *et al.* (2004) for the Global Network of Iran. By this way, our regional network will be linked to the Global Network of Iran.

Precise site coordinates were obtained using the GAMIT/GLOBK software packages (Herring 2002; King & Bock 2002). The classical three-step approach (Feigl *et al.* 1993; Dong *et al.* 1998) was applied. During the first step, daily solutions are computed from loose *a priori* constraints to all parameters (coordinates, orbital and Earth Orientation parameters) using the doubly differenced phase observations. 16 IGS stations were added to tie our local network to the ITRF2000 reference frame. The short-term precision of the solutions may be estimated by the repeatabilities corresponding to the rms of the independent daily solutions about their mean value. The horizontal repeatabilities was ∼1.7 mm in 2000 and ∼2.6 mm in 2002.

In a second step, a set of coordinates and velocities were estimated from the daily loosely constrained parameters (first step) as quasi-observations in a Kalman filter. The local quasi-observations were combined with quasi-observations at 150 globally distributed IGS stations. The daily global solutions are given by SOPAC from January 1995 to March 2002 (Bock *et al.* 1997) (solutions available at http://sopac.ucsd.edu). Monthly average global solutions were used during this time when no survey occurred. The last step was devoted to the estimation of a six-parameter transformation (Dong *et al.* 1998).

At first, GPS velocities and their 95 per cent confidence ellipses are estimated in ITRF2000. Following McClusky *et al.* (2000) and Vernant *et al.* (2004), we define a stable European reference frame by minimizing the velocities of 16 IGS stations located in Western Europe and Central Asia (see Table 1 in Vernant *et al.* (2004), pole coordinates 56.11 ± 1.4°N, −100.79 ± 1.9°E, rate 0.26 ± 0.01° Myr^{-1} in ITRF2000 frame). We took into account the temporal and spatial correlation of the GPS noise (McClusky *et al.* 2000), by adding a coloured noise (random walk equal to 2 mm yr^{-1}) in estimating the velocities. The GPS velocities relative to ITRF2000 reference and Eurasia are given in Table 1. We chose the Arabia–Eurasia Euler vector published by Vernant *et al.* (2004) (27.9 ± 0.5°N, 19.5 ± 1.4°E, rate 1.41 ± 0.1° Myr^{-1}) to estimate the velocities in the Arabian reference plate. GPS velocities deduced from the GPS Global Network of Iran (sites LAMB, JASK, KHAS, ZABO, BAZM, CHAB, KERM, HARA, 1999 and 2001 campaigns) complete our local results (Vernant *et al.* 2004). The final GPS velocities with respect to Arabia are shown on Fig. 3 (see also Table 1). Very small changes are observed in the estimated velocities when Eulerian poles published by Sella *et al.* (2002) and McClusky *et al.* (2003) are used (rms of 0.5 mm yr^{-1} on the residual velocities).

4 GPS HORIZONTAL VELOCITY ANALYSIS

In the Eurasia fixed reference frame, velocities are uniformly oriented N 10° over the transition zone, as attested by the large north

Table 1. GPS site velocities and 1σ uncertainties. Longitude (Lon.) and Latitude (Lat.) are given in degrees east and north, respectively. Velocities and uncertainties in mm yr^{-1}. Following Vernant *et al.* (2004), the Eurasia frame is chosen by minimizing the adjustments to the horizontal velocities of 14 IGS stations located in Western Europe and characterized by *a priori* zero velocities. The *a priori* velocities of IGS stations POL2 and KIT3 are fixed to 2 mm yr^{-1} N and 0.5 mm yr^{-1} E.

Site	Lon.	Lat.	Velocity/Eurasia		Uncertainty		ρ^b	Velocity/Arabia		Velocity/ITRF2000	
	°E	°N	E vel.	N vel.	E σ^a	N σ^a		E vel.	N vel.	E vel.	N vel.
BAGH	55.657	27.000	5.14	24.77	2.08	1.79	0.030	0.90	1.00	33.52	30.90
BAZM	60.180	27.865	5.33	3.11	2.06	1.62	0.038	0.75	−23.15	33.60	8.28
CHAB	60.694	25.300	1.39	7.82	1.90	1.56	0.038	−4.94	−18.72	30.84	13.24
DENA	56.504	28.529	4.38	15.50	1.98	1.73	0.023	1.00	−8.75	32.85	21.30
FINO	55.867	27.651	1.79	19.73	2.04	1.78	0.026	−2.05	−4.16	30.22	25.76
GENO	56.162	27.366	4.25	21.70	2.04	1.79	0.027	0.16	−2.36	32.69	27.66
GHOL	57.217	28.010	2.06	16.27	1.90	1.67	0.029	−1.81	−8.38	30.46	22.04
HARA	54.608	30.079	1.99	15.88	1.72	1.52	0.033	0.05	−7.29	30.23	22.38
JASK	57.767	25.636	2.78	14.24	1.71	1.48	0.040	−2.77	−10.71	30.92	20.21
KERM	57.119	30.277	1.58	16.07	2.51	1.71	0.043	−0.75	−8.52	29.68	21.90
KHAS	56.233	26.208	5.22	24.40	1.94	1.56	0.036	0.34	0.30	33.21	30.49
LAMB	54.004	26.883	2.99	22.30	2.02	1.58	0.031	−1.02	−0.52	30.88	28.79
MINA	57.100	27.160	1.36	23.36	1.89	1.64	0.030	−3.05	−1.22	29.72	29.18
MOSH	57.620	26.993	1.21	14.26	1.93	1.69	0.029	−3.41	−10.61	29.48	20.02
POOS	57.237	26.379	2.58	24.18	2.01	1.75	0.029	−2.37	−0.48	30.83	30.07
RAZD	55.800	28.330	3.11	15.82	1.82	1.59	0.029	−0.26	−8.03	31.60	21.84
SARZ	56.946	27.488	−1.33	19.70	1.99	1.75	0.026	−5.49	−4.80	27.01	25.52
SORC	57.884	27.901	1.60	13.73	1.97	1.69	0.031	−2.47	−11.29	30.05	19.34
ZABO	62.517.	31.049	0.89	0.57	1.58	1.45	0.006	−2.70	−27.03	29.36	5.59

[a] 1σ uncertainties.
[b] Correlation coefficient between the east and the north uncertainties.

component of the velocities (Table 1). The HAJI velocity is not presented here because its trend is not consistent with the very close RADZ velocity. This discrepancy cannot be explained by the local tectonic conditions and is probably originated from the instability of the HAJI site during the 2000–2002 epoch. JASK is the single site belonging to the Global Network of Iran and to our network. Increasing and densifying the total length of GPS observation for JASK from 1999–2001 to 1999–2000-2001–2002 epoch does not change significantly the velocity estimated during the two epochs (see Table 1 and Vernant *et al.* 2004). Near the Strait of Hormuz, the site BAGH is characterized by a velocity of 25.3 ± 2 mm yr^{-1} consistent with velocities of 22.5 and 24.5 mm yr^{-1} estimated at sites LAMB and BAGH by Vernant *et al.* (2004) from GPS measurements in 1999 and 2001 of the Iran Global Network. From the coast (BAGH) to the MZT (DENA, RAZD), the rate of shortening is 9 ± 2 mm yr^{-1} as across Central Zagros (Tatar *et al.* 2002; Vernant *et al.* 2004). The velocity referenced to Eurasia decreases abruptly of 10 ± 3 mm yr^{-1} when crossing the ZMP faults between the west sites (MINA, POOS, SARZ) and the east sites (JASK, MOSH, GHOL) (Table 1). At 28°N of latitude, velocity on both sides of the JS faults vary from 16 ± 2 mm yr^{-1} at west (GHOL) to 13 ± 2 mm yr^{-1} at east (SORC).

In the Arabia fixed reference frame (Fig. 3a and Table 1), we observe very low velocities for the western Iranian coastal sites: LAMB, BAGH, and KHAS on the Musandam peninsula. Assuming a N160° trend for the ZMP faults, the GPS dextral strike-slip component is estimated at 4.6 mm yr^{-1} (SARZ–GHOL), 7.1 mm yr^{-1} (MINA–GHOL) and 9.4 mm yr^{-1}(JASK–POOS).

This strike-slip motion parallel to the fault system is accompanied by an increase of the component perpendicular to the fault from 1.3 mm yr^{-1} (MINA–GHOL), to 2.4 mm yr^{-1} (MOSH–MINA) and to 4.0 mm yr^{-1} (JASK–POOS). However, the orientation of the ZMP fault system is N140° in the northern area. If we adopt this orientation, the projected strike-slip and thrust components are 6.3 mm yr^{-1} and 3.6 mm yr^{-1}, respectively, between the sites MINA and GHOL.

From the velocities of the sites SORC and GHOL, we estimate 3.1 ± 2.5 mm yr^{-1} to be the total dextral strike-slip displacement along the north–south JS fault system. Velocities for the eastern coastal sites GENO, SARZ, MINA and POOS are 'radially oriented': the vectors point towards the strait of Hormuz with a maximum at SARZ (7.3 ± 2 mm yr^{1}) in a southwest direction. RAZD, DENA, HARA and KERM are characterized by a referenced Arabia velocity of 10 ± 2 mm yr^{-1} and belong to the southeast extremity of the rigid CIP on the base of the seismological observations (Fig. 1). We have tested this assumption by using the Euler pole of the CIP relative to Eurasia published by Vernant *et al.* (2004) (23.15 ± 13.2°N, 0.98 ± 1.2°E, rate 0.189 ± 0.1°Myr^{-1}). The residual velocities are within the 1σ uncertainties and indicate a small deformation at the SE end of the CIP. We also confirm the eastward increase of the N10° trending shortening rate along the Makran subduction, from 11 ± 2 mm yr^{-1} for JASK at the western end of the accretionary wedge to 19 ± 2 mm yr^{-1} for CHAH.

5 DISCUSSION

The study area corresponds to a major tectonic discontinuity between the Eastern Zagros mountains and the oceanic Makran subduction zone which accommodate about 50 per cent and 80 per cent, respectively, of the Arabia–Eurasia convergence. In order to better understand the distribution of the horizontal deformation, we adopt a continuous approach to describe the strain rates over the transition zone, being aware of the limits of such assumption when the deformation is localized along faults, as for instance the ZMP fault or JS fault systems. The principal strain rate axes and the rotation rates have been calculated within each triangle from the velocities observed in the corners (Figs 4a and b).

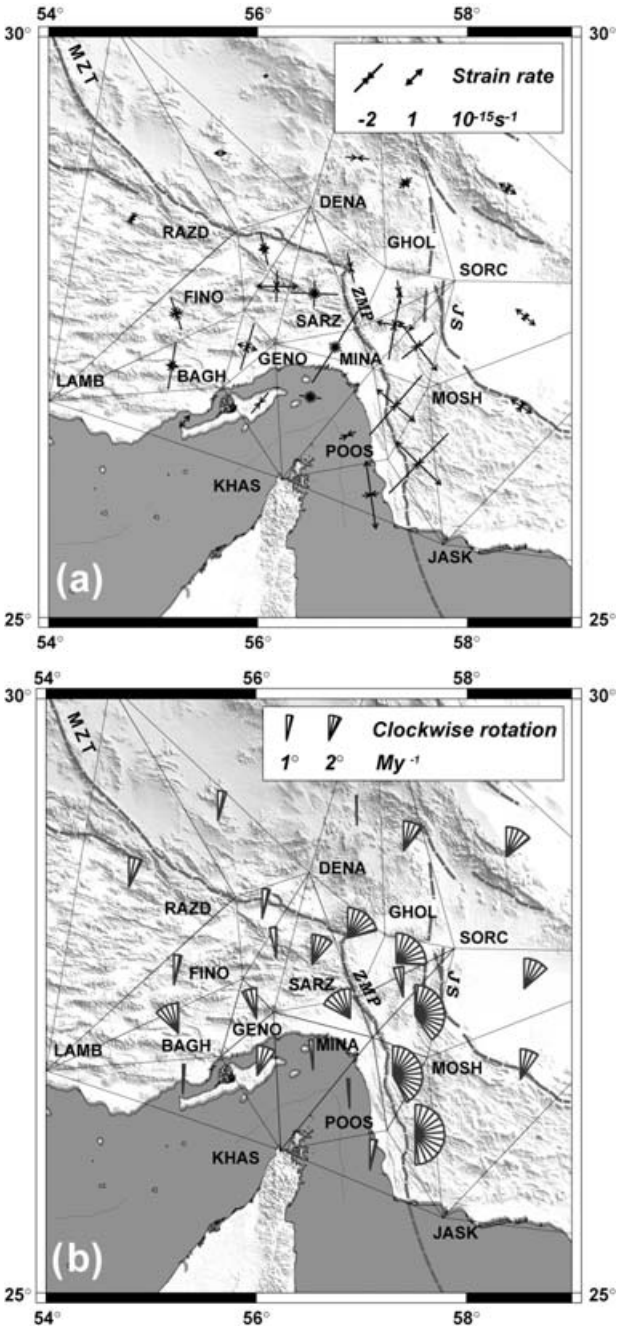

Figure 4. Strain rates and rotations. The principal strain rate axes (a) and the rotation rate (b) have been calculated at the centre of each triangle from the velocities observed at the corners.

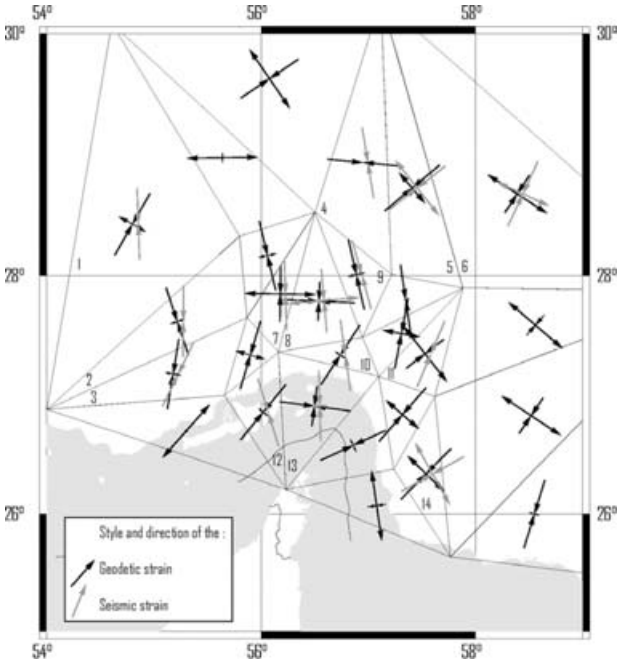

Figure 5. Principal horizontal axes of the geodetic (black arrows) and seismic (grey arrows) strain rate tensor to compare the direction and style of the seismic and geodetic strain rate fields. Amplitudes are normalized.

Comparison of the seismic, geodetic and tectonic deformation is important for better understanding the style, direction and rate of geological deformation. This approach may be critical since strain rates estimated from earthquake focal mechanisms and GPS velocities are not representative of long-term tectonic deformation, particularly for large active faults. Seismic and geodetic deformation may be compared to estimate the seismic/geodetic strain rate. This ratio was quantified in Iran and Zagros by Jackson & McKenzie (1988) using instrumental and historical seismicity and plate kinematic models. Masson *et al.* (2005) have recently reestimated this ratio using geodetic strain rates estimated from available GPS data in Iran (Vernant *et al.* 2004). Densifying the GPS sites in the Zagros Makran transfer zone in this work offered a good opportunity to compare style and direction of the geodetic and seismic strain rates. This is particularly interesting for the Zagros fold and thrust belt where earthquakes are mainly localized in the basement whereas geodetic velocities could be rather representative of motion within the sedimentary cover.

The method of analysis was formulated by Jackson & McKenzie (1988) and we refer to Kostrov (1974) for a complete formulation of the relationship between average seismic strain rate tensor and moment tensors of earthquakes occurring in a volume containing active faults. A thickness of 15 km for seismogenic layer is adopted from focal depth estimates (Jackson & McKenzie 1988; Hatzfeld *et al.* 2003). We take a modulus of rigidity of 3×10^{10} Pa. The seismic strain rate is computed for each triangle shown in Fig. 4, using earthquakes from the Harvard centroid moment tensor catalogue for the time period 1976–2004 (depth of earthquakes <15 km). Because we use a relatively small earthquake data set, Fig. 5 shows geodetic and seismic strain rate axes normalized to the maximum value. This representation allows a comparison of the direction and style of the geodetic and seismic strains, even if the seismic strain is small. In most of the triangles the fix and style of the geodetic and seismic strains are roughly similar. This agreement is particularly noticeable in Zagros (triangles 2, 3, 7, 8), in the JS fault system area (5, 6) and along the ZMP fault system (14). Around the Hormuz Strait a more complex pattern is observed. While the geodetic compressive strain is rotated eastwards, the seismic strain indicates mainly a NS compressive component (10, 11, 12, 13).

The Arabian plate is weakly deformed beneath the Persian gulf as attested by the very low deformation of triangles LAMB–BAGH–KHAS and BAGH–GENO–KHAS. Shortening of the sedimentary cover is mainly accommodated in the Zagros fold belt by an arcuate pattern of folds. Balanced cross-sections across the highly

deformed sedimentary cover in Central Zagros yield a NE-trending shortening rate of 10 mm yr^{-1} since 5 Ma (Blanc *et al.* 2003), in agreement with our estimation for the present-day shortening velocity. The NS orientation of the geodetic compressive strain axes are roughly perpendicular to the fold axes (Fig. 4a). The consistency between the geodetic and seismic strain rate tensors in Zagros (see triangles 2, 3, 7, 8 in Fig. 5) indicates a strong mechanical coupling between the folded and thrusted sedimentary cover and the basement. Many authors pointed out the role of the basement strike-slip faults in the building of the Zagros folds (Berberian 1995; Hessami *et al.* 2001). In the SE Zagros, Hessami *et al.* (2001) have depicted two strike-slip fault systems implying that fault-bounded basement blocks and cover may have rotated anticlockwise in the northern part and clockwise in the southern part. The anticlockwise rotations observed for the triangles LAMB–FINO–BAGH, BAGH–FINO–GENO and GENO–SARZ–MINA (Fig. 4b) do not confirm such a hypothesis. In the same area, Aubourg *et al.* (2004) emphasized the sigmoidal shape of the post Miocene folds (Fig. 2) and explained this trend by the existence of an offshore NE-trending left-lateral shear band. Our geodetic survey gives no evidence for such a deformation over the Strait of Hormuz (Fig. 3 and Fig. 4a).

Further East of the Zagros, towards the ZMP and JS fault systems, a rotation of the compressive axis is identified from a roughly NS Zagros orientation to a N45° compressive strain regime (Figs 4a and 5). This shortening fan shaped pattern is also revealed by the orientation of the Neogene and younger folds along the coast line (Fig. 2) and the magnetic fabric of weakly deformed sedimentary rocks from Zagros–Makran zone (Aubourg *et al.* 2004): the anisotropy of magnetic susceptibility (AMS) shortening direction varies from N350°W in the SE Zagros to N60° towards the Makran zone. The velocities at GENO, SARZ, MINA and POOS are perpendicular to the Neogene and younger fold axes along the coast line and predict compressive structures in the eastern part of the Strait of Hormuz. From sandbox experiments, Dominguez *et al.* (2000) have analysed stress and deformation of accretionary wedges in response to seamount subduction. They showed that the indentation of the margin occurs above the leading slope of the seamount. Conjugate shear zones associated with strike-slip faults trending oblique to the direction of convergence suggest that compressive stress axes $\sigma 1$ converges in the wake of the seamount whereas extensional stress axes $\sigma 3$ tend to parallel the relative plate motion in the wake of the seamount (see Fig. 10 in Dominguez *et al.* 2000). The NNE-trending structures of the Musandam mountains could act as an 'elongated seamount' subducting beneath the strait of Hormuz in the N10° direction. Therefore, the topography of the Musandam could be the cause of the margin reentrant, as attested by the curvature of the Iranian coastal line and fold axes. This model could also explain the sigmoidal shape of the folds in the southeastern part of the Zagros (Aubourg *et al.* 2004) and the orientation of compressional axes observed by AMS technique (Aubourg *et al.* 2004) and by GPS.

Along the ZMP fault system, large clockwise rotations (4–6° Ma^{-1}) and strain rates (3–4 10^{-15} s^{-1}) are assumed to be lower bounds since the deformation is located over a band width less than 20 km (Fig. 3b). Both strain axes and infinitesimal rotations clearly illustrate the major part of the dextral strike-slip component of the present day motion along the ZMP fault system. Such a result is not compatible with a present-day purely dip-slip movement predicted for the Zendan fault by Molinaro *et al.* (2005). The N45° compressive strain is in agreement with the N60° trend of the seismic compressive component (see triangle 14 in Fig. 15) and the N45° direction of the σ_1 stress axis direction estimated by Regard *et al.* (2004) from fault-slip vector analyses along the ZMP fault system. The transpressive character of the present-day tectonic regime evocated by Regard *et al.* (2004) is consistent with the distribution of the velocities at sites near the ZMP fault system (Fig. 3): the obliquity of the N10° trending velocity field in the western Makran with respect to the N160° or N140° strikes of the ZMP fault system may generate a displacement perpendicular to the faults. We have shown that the strike-slip motion increases southwards and could be distributed over a large area where the Zendan and Palami faults split in several fault zones around the Jask region (Fig. 2). Regard *et al.* (2005) propose that the northern part of ZMP fault system accommodates a convergence velocity of 5.6 ± 2.3 or 7.4 ± 2.7 mm yr^{-1} in the direction N11 ± 24° or N13 ± 26°, depending on the shear rate considered for the Zendan fault. They estimate the mean shortening along the northern ZMP fault system to be ∼1 mm yr^{-1}. Following the GPS results, this shortening is underestimated and may reach ∼3 mm yr^{-1}. The purely strike-slip motion observed between SARZ and GHOL is not in contradiction with the existence of a reverse component in this area since it is related to the deformation along the Zendan Palami faults. Shortening is clearly observed at SARZ site and may be partly accommodated by the Minab fault.

The ZMP fault zone is paradoxically aseismic in western Makran (Fig. 2). It is possible that the ZMP fault zone experiences aseismic creep at all times or is locked at the present day. In this case, the ZMP fault system could rupture over a large distance with a slip release corresponding to $Ms > 7$, if the last earthquake occurred as long ago as 1483 (Byrne *et al.* 1992). Molinaro *et al.* (2005) suggest that the basement is not involved in the deformation of the ZMP fault system. For these authors, the Zendan fault has a shallow low-angle geometry and accommodate mainly dip-slip movement. If the geodetic velocity shows that the first order motion is right-lateral strike-slip for the ZMP system, we cannot exclude that the ZMP fault system could root eastwards as proposed by Molinaro *et al.* (2005).

We have used a block model (Meade *et al.* 2002; Meade & Hager 2005) to test the effects of a eastward-dipping fault system, and the depth of locking along the ZMP fault system. A very simple model is chosen consisting of three elastic blocks, the Arabian plate, the Central Iranian plateau and the Lut-Makran Block, separated by the MZT, the ZMP and JS fault systems and the southern limit of the Makran wedge. We assume that the MZT and the JS fault systems are vertical and the frontal thrust of the Makran wedge dips northwards at 45° (Ravaut *et al.* 1997). Our model does not attempt to model the strain distribution over the SE Zagros where the deformation is distributed over the belt. We will focus our analysis on the central part of the ZMP fault system, assuming that the models will be strongly dependent on the mechanical and geometrical properties of the ZMP fault system. The model includes the effect of block rotation and elastic strain accumulation consistent with a simple model of the earthquake cycle. We invert the geodetic data, including the GPS sites on the Arabian plate (Vernant *et al.* 2004), to compute the Euler vectors of rotation of the blocks. The fault-slip rate at the ZMP fault system boundary is given by the differential of motion between the Arabian plate and the Lut-Makran Block. Using Okada's (1985) solution, the interseismic elastic effect of each fault segment limiting the blocks is computed. The elastic deformation associated with the ZMP fault system depends on the dip and the locking depth of the faults. Locking depth of 15 km is chosen for all the other segments. Elastic strain associated with the ZMP fault system has been computed along a N70° trending profile located at 26.5°. We have tested various inclinations for the ZMP fault system and the results not presented here indicate that the measured fault parallel velocities cannot be explained by dips of less than

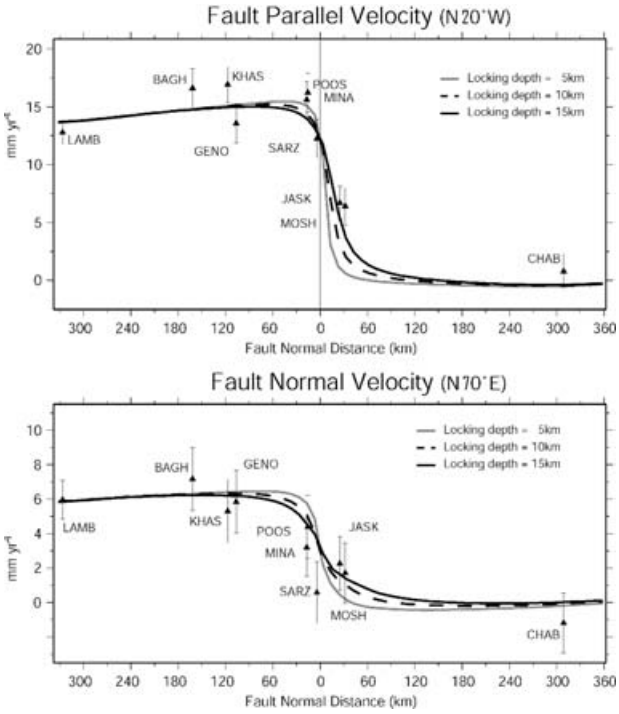

Figure 6. Fault-parallel and fault normal velocities to the ZMP fault system. The azimuth of the faults is N160°. The observed velocities presented in Table 1 have been projected onto a N70° trending profile crossing the ZMP faults at 26.5°N. We use a block model approach (Meade *et al.* 2002; Meade & Hager 2005) to estimate secular fault-slip rate, geometry and locking depth of the ZMP fault system. We assume that the ZMP faults accommodate the motion between the Arabian plate and the Makran–Lut Block. The block model takes into account the effects of the block rotation and elastic strain accumulation on the velocity. The theoretical velocities are estimated for faults dipping to the east with an inclination of 45°. The plotted curves correspond to locking depth of 5, 10 and 15 km.

30°. Fig. 6 shows the elastic strain for locking depths of 5, 10 and 15 km and a dip angle of 45°. The adopted model assumes that the ZMP fault system transfers the deformation between the Arabian plate and the Lut-Makran block. The model suggests that the long-term transpressive deformation along the ZMP faults accommodates a dextral strike-slip motion of 15 mm yr^{-1} and a shortening of 6 mm yr^{-1} between the two blocks. The model does not take into account the anelastic permanent deformation (for instance folds in the Makran prism), and the estimated velocities are considered as upper bounds. These high values reconcile the EW increase of the velocity between JASK and CHAB as a consequence of the elastic strain accumulation associated with the ZMP fault system. Locking depths of 10–15 km are consistent with the GPS velocities (see for instance sites MOSH and JASK).

The 3.1 $\pm$ 2.5 mm yr^{-1} dextral strike-slip motion along the JS fault system results only from SORC and GHOL sites and, therefore, suffers from large uncertainty. Nevertheless, this result is apparently consistent with the 1.5–2.4 mm yr^{-1} velocity for the NG fault system (Walker & Jackson 2002). However, the displacement has been estimated, respectively, at 50 km (GHOL) and 10 km (SORC) on both sides of the JS fault system. Assuming that JS fault system is presently locked, we estimate an interseismic loading rate probably lower than the long-term rate of the strike-slip motion. Therefore, our result does not conflict with the 5.7 $\pm$ 1.7 mm yr^{-1} slip rate estimated by Regard *et al.* (2005).

Regard *et al.* (2005) evaluate the global velocity between the Musandam peninsula and the Jaz Murian to 11.2 $\pm$ 3.9 or 13.0 $\pm$ 3.9 mm yr^{-1} with a N10° trending. It is paradoxical that this estimation is lower than the 15mm yr^{-1} given by the block model for the ZMP fault system only. We propose here a simpler explanation assuming that the shear velocity along the ZMP increases southwards from the MZT to the western Makran: the northern fault segments analysed by Regard *et al.* (2005) are roughly oriented N140° resulting in a lower strike-slip motion. The GPS right-lateral strike-slip velocities of GOHL with respect to SARZ (5.1 $\pm$ 2 mm yr^{-1}) and MINA (6.3 $\pm$ 2 mm yr^{-1}) confirm this assumption.

The tectonic setting in the ZMP transfer zone differs from the JS fault system as it connects the Zagros and Makran wedges whereas the JS one and its northward prolongation, the NG fault system, transfers some deformation from the Makran subduction to the north of Iran. How can we explain the large differential motion along the ZMP fault system? We have proposed previously the possible role of the Musandam Peninsula acting as an indenter of the Arabia into the Iranian crust. Moreover, simultaneous deformation of the continental and oceanic accretionary prisms is partly governed by the frictional property of their associated substrates. Lateral variations in the rheology of the detachments beneath the prisms could result in differential propagation of the deformation front (Cotton & Koyi 2000). Experimental models suggest inflection of the deformation front as a consequence of a faster propagation above a ductile substrate relative to a frictional substrate. Inflection is also accompanied by formation of transpressive folds and faults (see Fig. 12 in Cotton & Koyi 2000). Also, the Makran zone is characterized by a large amount of unconsolidated and saturated water sediments, which may result in a low apparent friction on the detachment and may also explain the aseismic behaviour of the western Makran (Byrne *et al.* 1992). However, our GPS results do not bring evidence of a rapid southward propagation of the Makran prism.

At a larger scale, the ZMP, the JS- NG and Neh–Zahedan fault systems transfer the shortening in Iran from the western part where the deformation is widely distributed from the Zagros mountains to the Caspian sea, to the East where the Makran subduction mostly accommodates the deformation.

The large width of the area affected by the fault systems could indicate that the underthrusting Arabian plate beneath the Makran and the Zagros zones is continuous (Regard *et al.* 2005). The east–west asymmetry in deformation of the Iranian lithosphere may be inherited from a stronger rigid behaviour of Lut and Helmand blocks. Also, localization of the deformation along the N–S fault systems may correspond to major lithospheric weakness almost parallel to the direction of convergence. Conversely, low oceanic–continental coupling may also reduce the compressive force exerted and deformation on the overriding plate (Vernant *et al.* 2004). It has been suggested that the strain in the overriding plate during a subduction process is strongly dependent on the coefficient of friction along the subduction plane and on the density contrast between lithosphere and asthenosphere (Hassani *et al.* 1997; Chemanda *et al.* 2000). The compressive force exerted on the overriding plate along the subducting plate depends on the effective friction force and the non-hydrostatic interplate pressure force. Low frictional coefficient is expected along the Makran subduction plane as it is probably controlled by lubrication of the weak sediments dragged between the plates. To the west, the continental collision in Zagros is accompanied by underthrusting and thickening of the Arabian continental crust. In this case, the lack of a well defined localization

zone may result in higher friction and mean stress. Consequently, the compressive stress may be transmitted through the rigid Central Iranian Block and would lead to localize the present-day deformation in northern Iran (Tabriz fault system, Alborz and Kopet Dagh mountains).

6 CONCLUSIONS

On the basis of the GPS observations reported in this paper, the deformation between the Zagros and Makran mainly corresponds to a transpressive regime, with a right-lateral strike-slip motion close to the ZMP fault zone at velocity of 10 ± 3 mm yr^{-1} which is the most important relative displacement rate observed by GPS on a single fault system in Iran. Using a simple block model, we have shown that the observed velocities are in agreement with a long-term motion between Arabian plate and the Makran–Lut Block of 15 mm yr^{-1} for the strike-slip component and 6 mm yr^{-1} for the shortening component on the ZMP fault system. This displacement is accompanied by right-lateral strike-slip motion along the JS fault zone at velocity of 3.1 ± 2.5 mm yr^{-1}. However, our GPS sites are too sparse to predict if the segments of the ZMP fault system are creeping aseismically or if they may rupture in large earthquakes ($Ms > 7$) with long recurrence times. Further GPS measurements on dense networks and INSAR investigations along the faults zone will allow us to address this question. We propose that the radial GPS velocities observed along the coastal line probably reflects the mechanical impact of the subducting Musandam Peninsula on the shortening fan pattern around the Strait of Hormuz.

At regional scale, the right-lateral motion along the ZMP may not be completely explained by local tectonic considerations. This fault system participates in the large dextral shear motion in eastern Iran, involving the JS–NG and Neh–Zahedan fault systems. These fault systems accommodate the shortening distributed on a broad deformation zone in the western Iran (Zagros, Alborz, Caspian sea, Kopet Dagh) whereas the convergence is mostly localized along the Makran subduction in the eastern part. Right-lateral strike-slip motion of NG and Neh–Zahedan fault systems remain poorly quantified and must be measured by GPS in order to better understand the distribution of right-lateral shear occurring on the borders of the Lut Block up to the Doruneh fault.

ACKNOWLEDGMENTS

This study was supported by INSU-CNRS (France) (program 'Intérieur de la Terre'), by the French Ministère des Affaires Etrangères and by the International Institute of Earthquake Engineering and Seimology (IIEES, Iran) in the frame of a co-operative research program. We thank the French Embassy for supporting this cooperative research program. We thank IIEES for fieldwork assistance and M. G. Ashtyani, president of IIEES who has supervised this work. We thank also M. Mokhtari for support and administrative assistance. The NCC have joined this study in 2002 by participating in the 2002 survey and we thank F. Tavakoli, director of the land-surveying and geodetic department of NCC for support. We thank also the NCC team of Bandar Abbas for field assistance. We are grateful to two anonymous reviewers who helped to improve the first version of the manuscript.

REFERENCES

Aubourg, C. *et al.*, 2004. Post-Miocene shortening pictured by magnetic fabric across the Zagros-Makran syntaxis (Iran), in eds Sussman, A.J. & Weil, A. B., *Orogenic curvature: Integrating paleomagnetic and structural analyses*, Boulder, Colorado, Geol. Soc. Am., special paper 383, 17–40.

Baker, C., Jackson, J. & Priestley, K., 1993. Earthquakes on the Kazerun line in the Zagros mountains of Iran: strike-slip faulting within a fold-an-thrust belt, *Geophys. J. Int.,* **115,** 41–61.

Berberian, M., 1995. Master 'blind' thrust faults hidden under the Zagros folds: active basement tectonics and surface morphotectonics, *Tectonophysics,* **241,** 193–224.

Blanc, E.J.-P., Allen, M.B., Inger, S. & Hassani, H., 2003. Structural styles in the Zagros Simple Folded Zone, Iran, *J. Geol. Soc. Lond.,* **160,** 401–412.

Bock, Y., Bear, J., Fang, P., Dean, J. & Leigh, R., 1997. Scripps Orbit and Permanent Array center (SOPAC) and Southern Californian Permanent Geodetic Array (PGGA), in The Global Positioning System for Geosciences, *Nat. Acad. Press*, Washington, DC, 55–61.

Byrne, D., Sykes, L.R. & Davis, D.M., 1992. Great thrust earthquakes and aseismic slip along the plate boundary of the Makran subduction zone, *J. geophys. Res.,* **97,** 449–478.

DeMets, C., Gordon, R.G., Argus, D.F. & Stein, S., 1990. Current plate motions, *Geophys. J. Int.,* **101,** 425–478.

Dominguez, S., Malavieille, J. & Lallemand, S.E., 2000. Deformation of accretionary wedges in response to seamount subduction: insights from sandbox experiments, *Tectonics,* **19**(1), 182–196.

Dong, D., Herring, T.A. & King, R.W., 1998. Estimating regional deformation from a combination of space and terrestrial geodetic data, *J. Geodyn.,* **72,** 200–211.

Engdahl, R., van der Hilst, R. & Buland, R., 1998. Global teleseismic earthquake relocalisation with improved travel times and procedures for depth determination, *Bull. seism. Soc. Am.,* **88,** 722–743.

Feigl, K.L. *et al.*, 1993. Space geodetic measurement of crustal deformation in central and southern California, *J. geophys. Res.,* **98,** 21 677–21 712.

Chemanda, A., Lallemand, S. & Bokun A., 2000. Strain partitioning and interpolate friction in oblique subduction zones: constraints provided by experimental modeling, *J. geophys. Res.,* **105,** 5567–5581.

Cotton, J.T. & Koyi, H.A., 2000. Modeling of thrust fronts above ductile and frictional detachments: application to structures in the Salt Range and Potwar Plateau, Pakistan, *Geol. soc. Am. Bull.,* **112,** 351–363.

Hassani, R., Jongmans, D. & Chéry, J., 1997. Study of plate deformation and stress in subduction processes using two-dimensional numerical models, *J. geophys. Res.,* **102,** 17951–17965.

Hatzfeld, D., Tatar, M., Priestley, K. & Ghafory-Ashtiany, M., 2003. Seismological constraints on the crustal structure beneath the Zagros mountain belt (Iran), *Geophys. J. Int.,* **155,** 403–410.

Herring, T.A., 2002. *GLOBK: Global Kalman filter VLBI and GPS analysis program, version 10.0*, Mass. Inst. of Technol., Cambridge.

Hessami, K., Koyi, H.A. & Talbot, C.J., 2001. The significance of the strike-slip faulting in the basement of the Zagros fold and thrust belt, *J. Petrol. Geol.*, **24(1),** 5–28.

Jackson, J. & Fitch, T., 1981. Basement faulting and the focal depths of the larger earthquakes in the Zagros mountains (Iran), *Geophys. J. R. astr. Soc.,* **64,** 561–586.

Jackson, J.A. & McKenzie, D.P., 1988. The relationship between plate motions and seismic tensors, and the rates of active deformation in the Mediterranean and Middle East, *Geophys. J. R. astr. Soc.,* **93,** 45–73.

Jackson, J., Haines, J. & Holt, W., 1994. A comparison of satellite laser ranging and seismicity data in the Aegean region, *Geophys. Res. Lett.,* **21,** 2849–2852.

Jackson, J., Haines, J. & Holt, W., 1995. The accommodation of Arabia-Eurasia plate convergence in Iran, *J. geophys. Res.,* **100,** 15 205–15 219.

Kadinsky-Cade, K. & Barazangi, M., 1982. Seismotectonics of the Southern Iran: the Oman Line, *Tectonics*, **1(5),** 389–412.

King, R.W. & Bock, Y., 2002. *Documentation for the GAMIT analysis software, release 10.0*, Mass. Inst. of Technol., Cambridge.

Kostrov, B., 1974. Seismic moment and energy of earthquakes and seismic flow of rock, Izv. Acad. Sci. USSR, *Phys. Solid Earth,* **1,** 23–40.

Masson, F., Chéry, J., Hatzfeld, D., Martinod, J., Vernant, P., Tavakoli, F. & Ghafory-Ashtiani, 2005. Seismic versus aseismic deformation in Iran inferred from earthquakes and geodetic data, *Geophys. J. Int.,* **160,** 217–226.

McClusky, S. *et al.*, 2000. Global Positioning System constraints on plate kinematics and dynamics in the eastern Mediterranean and Caucasus, *J. geophys. Res.,* **105,** 5695–5719.

McClusky, S., Reilinger, R., Mahmoud, S., Ben Sari, D. & Tealeb, A., 2003. GPS constraints on Africa (Nubia) and Arabia plate motions, *Geophys. J. Int.,* **155**, 126–138.

Meade, B.J. & Hager, B.H., 2005. Block models of crustal motion in the southern California constrained by GPS measurements, *J. geophys. Res.,* **110,** B03403, doi:10.1029/2004JB003209.

Meade, B.J., Hager, B.H., McClusky, S.C., Reilinger, R.E., Ergintav, S., Lenk, O., Barka, A. & Ozener, H., 2002. Estimates of seismic potential in the Marmara Sea region from block models of secular deformation constrained by Global Postioning System measurements, *Bull. seism. Soc. Am.,* **92,** 208–215.

Molinaro, M., Guezou, J.C., Leturmy, P., Eshraghi, S.A. & Frizon de Lamotte, D., 2005. The origin of changes in structural style across the Bandar Abbas syntaxis, SE Zagros (Iran), *Marine and Petroleum Geology,* **21**(6), 735–752.

Okada, Y., 1985. Surface deformation due to shear and tensile faults in a half space, *Bull. seism. Soc. Am.,* **75,** 1135–1154.

Ravaut, P., Bayer, R., Hassani, R., Rousset, D. & Al Yahya'ey, A., 1997. Structure and evolution of the Northern Oman margin: gravity and seismic contstaints over the Zagros-Makran-Oman collision zone, *Tectonophysics,* **279,** 253–280.

Ravaut, P., Carbon, D., Ritz, J.F., Bayer, R. & Philip, H., 1998. The Sohar basin, Western Gulf of Oman: description and mechanisms of formation from seismic and gravity data, *Marine and Petroleum Geology.,* **15,** 359–377.

Regard, V., Bellier, O., Thomas, J.C., Abbassi, M., Mercier, J.L., Shabanian, E., Feghhi, Kh. & Soleymaani], Sh., 2004. The accommodation of the Arabia-Asia convergence in the Zagros-Makran transfer zone, SE Iran : a transition between collision and subduction through a young deforming system, *Tectonics,* **23,** TC4007, doi:10.1029/2003TC001599.

Regard, V. *et al.*, 2005. Cumulative right-lateral fault slip rate across the Zagros-Makran transfer zone: role of the Minab-Zendan fault system in accommodating Arabia-Eurasia convergence in southeast Iran, *Geophys. J. Int.,* **162,** 177–203.

Savage, J. & Burford, R., 1973. Geodetic determination of relative plate motion in Central California, *J. geophys. Res.,* **95,** 4873–4879.

Sella, G.F., Dixon, T.H. & Mao, A., 2002. REVEL: a model for Recent plate velocities from space geodesy, *J. geophys. Res.,* **107(B4),** doi: 10.1029/2000JB000033.

Tatar, M., Hatzfeld, D., Martinod, J., Walpersdorf, A., Ghafori-Ashtiany, M. & Chéry, J., 2002. The present-day deformation of the Central Zagros from GPS measurements, *Geophys. Res. Lett.,* **29**(19), 1927, 2002GL015427.

Vernant, P. *et al.*, 2004. Present-day crustal deformation and plate kinematics in the Middle East constrained by GPS measurements in Iran and Northern Oman, *Geophys. J. Int.,* **157,** 381–398.

Walker, R. & Jackson, J., 2002. Offset and evolution of the Gowk fault, SE Iran; a major intra-continental strike-slip system, *J. Struct. Geol.,* **24,** 1677–1698.

Yamini Fard, F., Hatzfeld, D., Mokhtari, M. & Farahbod, A.M., 2003. Microseismicity and crustal structure of the transition zone Zagros-Makran based on the data of a local dense temporary network, *proceedings, SEE4 Conference*, 12–14 may 2003, Tehran, Iran.